Sensitivity of (multi)fractal eigenstates to a perturbation of the Hamiltonian

M. A. Skvortsov [1] M. Amini [2] and V. E. Kravtsov[1,3]

[1]*L. D. Landau Institute for Theoretical Physics, Chernogolovka 142432, Russia*
[2]*Department of Physics, University of Isfahan, Hezar Jerib, 81746-73441 Isfahan, Iran*
[3]*Abdus Salam International Center for Theoretical Physics, Strada Costiera 11, 34151 Trieste, Italy*

We study the response of an isolated quantum system governed by the Hamiltonian drawn from the Gaussian Rosenzweig-Porter random matrix ensemble to a perturbation controlled by a small parameter. We focus on the density of states, local density of states, and the eigenfunction amplitude overlap correlation functions which are calculated exactly using the mapping to the supersymmetric nonlinear sigma model. We show that the susceptibility of eigenfunction fidelity to the parameter of perturbation can be expressed in terms of these correlation functions and is strongly peaked at the localization transition: It is independent of the effective disorder strength in the ergodic phase, grows exponentially with increasing disorder in the fractal phase, and decreases exponentially in the localized phase. As a function of the matrix size, the fidelity susceptibility remains constant in the ergodic phase and increases in the fractal and in the localized phases at modestly strong disorder. We show that there is a critical disorder strength inside the insulating phase such that for disorder stronger than the critical, the fidelity susceptibility decreases with increasing the system size. The overall behavior is very similar to the one observed numerically in a recent work by Sels and Polkovnikov [Phys. Rev. E **104**, 054105 (2021)] for the normalized fidelity susceptibility in a disordered XXZ spin chain.

I. INTRODUCTION

Parametric statistics is a general term for the response of a disordered quantum system to the variation of parameters of a Hamiltonian. In the case of the classical Wigner-Dyson random matrix theory (RMT) [1], one is usually interested in the *spectral response* to the parameter variation—the best-known examples are the so-called level velocity $dE_n/d\lambda$ and the level curvature $d^2E_n/d\lambda^2$ [2–9], where $E_n(\lambda)$ is the nth eigenvalue of the Hamiltonian

$$\widehat{H}(\lambda) = \widehat{H}_1 \cos\lambda + \widehat{H}_2 \sin\lambda, \tag{1}$$

in which $\widehat{H}_1$ and $\widehat{H}_2$ are drawn from certain disorder ensembles and λ is a parameter.

For the diffusive dynamics beyond the classical RMT, the parametric density of states (DoS) correlation function and the level curvature distribution in the crossover between the orthogonal and unitary ensemble was studied in Refs. [13,14] using the formalism of the supersymmetric nonlinear sigma model (NLSM) [15]. The dynamics of eigenvalues with λ, which plays a role of time, is sensitive to the Anderson localization and is a generalization of the Dyson's Brownian motion [16] of the gas of energy levels (Pechukas gas [17]) in the classical RMT. In the delocalized phase, it exhibits the avoided crossing of the word lines of energy levels as functions of λ, and in the localized phase the crossing is sharp.

The dynamics of the Pechukas gas is very peculiar if the wave functions are extended but not ergodic, obeying the multifractal statistics [18] (as, e.g., in the point of Anderson transition). The connection between this dynamics and the eigenfunction statistics [19] allowed us to derive a nontrivial relationship between the level compressibility χ and the fractal dimension D_q of eigenfunctions [20].

This incomplete review of old results shows that quite a bit is known about the spectral parametric statistics. However, by now information on the parametric statistics of *eigenfunctions*, especially for the multifractal case, is still lacking.

At the same time, the multifractal eigenfunction statistics appears to be quite ubiquitous. Not only is it common to critical points of Anderson transitions in noninteracting systems, a mounting evidence has emerged recently [21,22] that the many-body localized (MBL) phase in interacting systems is a phase with multifractal statistics of eigenfunctions in the Hilbert space.

Recently, the nonergodic extended (NEE) phase with fractal eigenfunction statistics has been shown [23] to emerge in the simplest extension of the Wigner-Dyson (WD) theory, the Gaussian Rosenzweig-Porter (GRP) random matrix ensemble [24]. Like in the classical RMT, all matrix entries in this ensemble are Gaussian random variables fluctuating independently of each other around zero with the variance that is identical for all the diagonal and off-diagonal matrix elements. The crucial difference is that the variance of the off-diagonal matrix elements is parametrically smaller than that of the diagonal ones and it decreases as a certain power $N^{-\gamma}$ of the matrix size N, while the variance of diagonal entries is chosen to be 1. This breaks the basis-rotation invariance of the classical RMT and allows for the nonergodic phases to emerge in the thermodynamic limit in the special basis in which the model is formulated.

Despite its quite specific formulation, this random matrix ensemble appears to have a predictive power even for the MBL transition in interacting systems such as dirty bosons and spin chains [22]. A particular case of this model arises also in the quantum random energy problem [25,26], which has important applications in quantum computing [25]. The Rosenzweig-Porter model with logarithmically normal distribution of off-diagonal entries (LN-RP) [27] has a particularly rich two-parameter phase diagram [10,11]. It has been shown [11] that at a certain relationship between the typical value and the variance of the log-normal distribution LN-RP model belongs to the same universality class as the Anderson model on random regular graphs (RRG). The latter model is often considered as a toy model for MBL [28–30].

Given a simplicity of the GRP model, in this paper we study the parametric statistics of local operators in this model with the goal of identifying the generic features intrinsic to all random systems in its multifractal phase.

II. TARGET PROPERTIES AND REVIEW OF MAIN RESULTS

Statistical properties of a quantum system are naturally described by the DoS and local DoS (LDoS) pair correlation functions:

$$R_E(\omega, \lambda) = \delta^2 \left\langle \sum_{n,m} \delta\left(E - E_n^{(0)}\right)\delta\left(E + \omega - E_m^{(\lambda)}\right)\right\rangle, \quad (2)$$

$$C_E(\omega, \lambda) = (N\delta)^2 \left\langle \sum_{n,m} \rho_n^{(0)}(r)\rho_m^{(\lambda)}(r) \right.$$
$$\left. \times \delta\left(E - E_n^{(0)}\right)\delta\left(E + \omega - E_m^{(\lambda)}\right)\right\rangle, \quad (3)$$

where N is the dimension of the Hilbert space (size of an $N \times N$ random matrix), δ is the mean level spacing at the band center, $\rho_m^{(\lambda)}(r) = |\Psi_m^{(\lambda)}(r)|^2$ is the density operator, $\Psi_n^{(\lambda)}(r) = \langle r|n(\lambda)\rangle$ is the nth eigenfunction of the Hamiltonian (1) corresponding to the parameter λ at a point r, and $E_n^{(\lambda)}$ is the corresponding eigenvalue. Angular brackets $\langle \ldots \rangle$ stand for disorder average.

Since the dependence of the correlation functions (2) and (3) on the reference energy E is very slow, one typically considers them at the band center. That will be implied throughout the text, so we will suppress the subscript E: $R(\omega, \lambda) \equiv R_0(\omega, \lambda)$ and $C(\omega, \lambda) \equiv C_0(\omega, \lambda)$.

While the DoS correlator $R(\omega, \lambda)$ is determined only by the eigenvalues, the LDoS correlator $C(\omega, \lambda)$ also encodes information about the eigenfunctions. In many cases, the spectrum and eigenfunctions are uncorrelated. The best-known examples are the classical RMT [1] (fully ergodic states) and random diagonal matrices (perfectly localized states). Then the function $C(\omega, \lambda)$ reproduces level repulsion features of the DoS correlator $R(\omega, \lambda)$ and it is instructive to focus on their ratio [31]:

$$K(\omega, \lambda) = \frac{C(\omega, \lambda)}{R(\omega, \lambda)}. \quad (4)$$

We will show that for the GRP model, $K(\omega, \lambda)$, indeed, coincides, in its principal detail, with the correlation function of

the density operators:

$$\tilde{K}(\omega, \lambda) = N^2 \langle \rho_m^{(0)}(r)\, \rho_n^{(\lambda)}(r)\rangle, \quad E_n - E_m = \omega \quad (5)$$

(both E_n and E_m taken close to the band center). For this reason, the correlation function $K(\omega, \lambda)$ will be referred to as the eigenfunction amplitude overlap (EAO) correlation function.

In this paper, we consider three types of perturbations $\widehat{H}_2$ in Eq. (1): (i) the diagonal drive when $\widehat{H}_2$ is the diagonal part of the RP random matrix, (ii) the off-diagonal drive when $\widehat{H}_2$ is the off-diagonal part of this matrix, and (iii) the local density drive $\widehat{H}_2 = (N\delta)\,|r\rangle\,\langle r|$.

The main effect of the *diagonal drive* is a random shift Δ of the entire miniband [32] of the nearly resonant states in the local spectrum following the shift of the matrix element $H_{r,r}$ [see Fig. 1(a)]. In the case of the *off-diagonal drive*, the miniband does not move as a whole. However, in both cases (i) and (ii), the individual levels do move. At a small perturbation strength λ, the shift of a single level manifests itself in $K(\omega, \lambda)$ as the broadening of the self-correlation δ peak in $K(\omega, 0)$. The second effect of perturbation is the suppression of level repulsion seen as a correlation hole in $C(\omega, \lambda)$ and $R(\omega, \lambda)$ at $\omega \lesssim \delta$, see Fig. 2.

The point of a special focus in this paper is the *fidelity susceptibility* [33–35] characterizing the overlap of the bare and perturbed wave functions averaged over all states:

$$\chi_F = -\partial_{\lambda^2} \frac{1}{N} \sum_n \left|\langle \Psi_n^{(0)}|\Psi_n^{(\lambda)}\rangle\right|^2_{\lambda=0}. \quad (6)$$

For a generic perturbation $\widehat{H}_2$, the fidelity susceptibility bears information on quantum phases. We consider the specific case of the local density drive $\widehat{H}_2 = (N\delta)\,|r\rangle\,\langle r|$ when the respective χ_F is insensitive to phases of eigenfunctions and can be expressed via the correlation function $C(\omega, 0)$. We show that the *typical* fidelity susceptibility for the local density drive in the GRP ensemble is given by

$$\chi_F^{(\text{typ})} \sim C(\delta, 0) \sim K(\delta, 0). \quad (7)$$

One of the main results of the paper is the exponential growth of the typical fidelity susceptibility $\chi_F^{(\text{typ})} \sim N^{\gamma-1}$ as a function of the disorder parameter γ in the fractal NEE phase ($1 < \gamma < 2$). This result is derived analytically and confirmed numerically. In the ergodic phase ($\gamma < 1$), the susceptibility $\chi_F^{(\text{typ})}$ is independent of γ and is much smaller than in the NEE phase, while in the localized phase ($\gamma > 2$) it exponentially decreases as $N^{3-\gamma}$ with increasing γ, see Fig. 1(b). The maximum of $\chi_F^{(\text{typ})}(\gamma)$ in the limit of large N is located exactly at the localization transition $\gamma = 2$.

An important feature of the dependence of $\ln \chi_F^{(\text{typ})}$ on γ in the GRP model is a symmetric character of this dependence with respect to the Anderson transition point $\gamma = 2$, see Fig. 1(b). It is instructive to compare this behavior with the one for the log-normal RP model [27] which is equivalent to the Anderson localization model on RRG [10,11]. In that case, the NEE phase is only a finite-size effect, which manifests itself in the *asymmetric* shape of the dependence of $\ln \chi_F^{(\text{typ})}$ on γ, see Fig. 1(c). With increasing the matrix size N, the asymmetry grows and in the limit of an infinite system one obtains a discontinuous curve for $\mu(\gamma) = d \ln \chi_F^{(\text{typ})}/d \ln N$
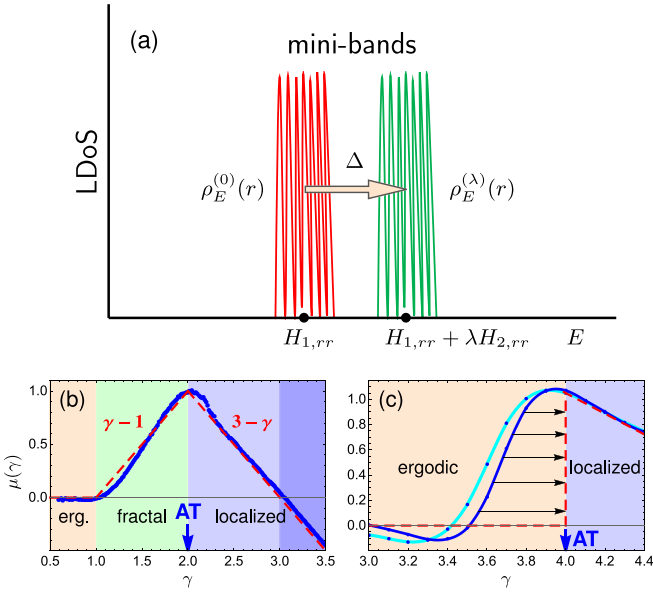
FIG. 1. Main results. (a) Schematic shift of an entire miniband of the width Γ in the spectrum of LDoS, $\rho_E^{(\lambda)}(r) = \sum_n |\Psi_n^{(\lambda)}(r)|^2 \delta(E - E_n^{(\lambda)})$, consisting of a macroscopic number of states, caused by a parametric shift of a diagonal matrix element H_{rr} corresponding to the observation point r. (b) The logarithmic derivative, $\mu(\gamma) = d \ln \chi_F^{(\text{typ})} / d \ln N$, of the typical fidelity susceptibility $\chi_F^{(\text{typ})} \sim K(\delta, 0)$ as a function of the effective disorder parameter γ [defined in Eq. (10)] for the Gaussian Rosenzweig-Porter (GRP) model in its ergodic, fractal, and localized phases. Blue points are the results of exact diagonalization of corresponding random matrices [shown is the discrete derivative $d \ln K(\delta, 0)/d \ln N$ between $N = 1024$ and $N = 2048$]. The red, dashed, *symmetric* with respect to the Anderson transition (AT) point $\gamma = 2$ curve is the analytical prediction. The fractal phase at $1 < \gamma < 2$ manifests itself in the exponential growth $\propto N^{\gamma-1}$ of the typical fidelity susceptibility as a function of γ (and power-law growth as a function of N). The fidelity susceptibility has a maximum at the localization transition at $\gamma = 2$. In the localized phase, the susceptibility $\propto N^{3-\gamma}$ decreases as a function of γ but as a function of N it shows a peculiar behavior. It grows with N for $2 < \gamma < 3$ and decreases with N for $\gamma > 3$. In the limit $N \to \infty$, it is infinite for $2 < \gamma < 3$ (light blue filling) and zero if $\gamma > 3$ (dense blue filling). Thus, there exist two localized phases with drastically different responses to a local perturbation. The susceptibility in the ergodic phase is small and independent of γ. (c) The same logarithmic derivative $\mu(\gamma)$ as a function of γ for the Rosenzweig-Porter model with log-normal distribution of off-diagonal matrix elements (LN-RP) in the symmetric point $p = 1$ which is equivalent to the Anderson localization model on random regular graph (RRG) [10,11]. In this model, the fractal phase does not exist. As a result, the typical fidelity susceptibility evolves with increasing N to a *highly asymmetric* discontinuous curve shown by a red dashed line. The blue lines correspond to numerical diagonalization of random matrices drawn from LN-RP, $p = 1$ ensemble with $N = 4096, 8192$ (cyan), and $N = 8192, 16384$ (blue), and taking the discrete derivative with respect to $\ln N$. Very similar curves are obtained for the Anderson model on RRG and for the Heisenberg spin-1/2 chain in a random field [12].

versus γ shown by the red dashed line in Fig. 1(c). A very similar behavior has been obtained in Ref. [12] for the EAO correlation function of neighboring eigenstates in RRG and in
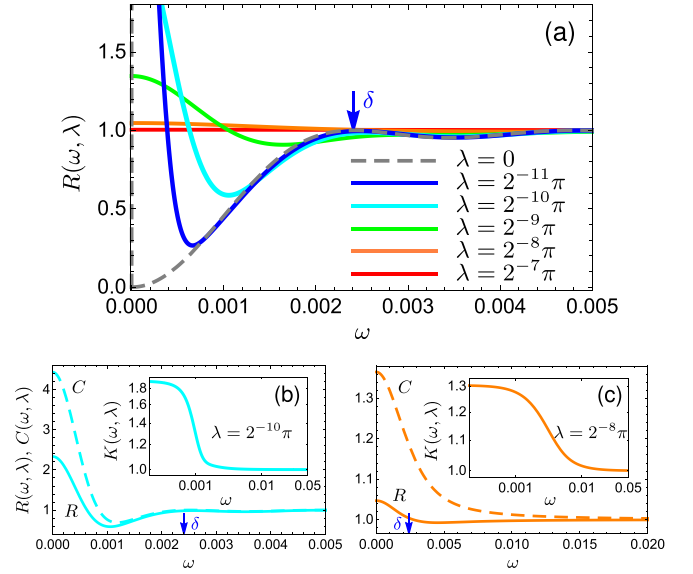

FIG. 2. Correlation functions $R(\omega, \lambda)$, $C(\omega, \lambda)$, $K(\omega, \lambda)$ for the unitary GRP ensemble in the fractal phase $\gamma = 3/2$ at $\Gamma/\delta = 32$ and $\delta = 0.0024$ in the large-N limit. The plots are obtained analytically from Eqs. (56), (61), (62). (a) Evolution of the DoS correlation function $R(\omega, \lambda)$ with increasing the parameter λ in Eq. (1). (b), (c) The correlation functions $R(\omega, \lambda)$, $C(\omega, \lambda)$, $K(\omega, \lambda)$ at $\lambda = \pi/1024$ and $\lambda = \pi/256$, respectively. The δ peak of level self-correlation is progressively broadened and the level repulsion correlation hole diminishes in $R(\omega, \lambda)$ and $C(\omega, \lambda)$ as λ increases. The eigenfunction amplitude overlap (EAO) correlation function $K(\omega, \lambda)$ demonstrates the broadened eigenfunction self-correlation peak rectified for the eigenvalue correlations.

the random-field spin-1/2 Heisenberg chain (cf. right panels of Figs. 3 and 6 in Ref. [12]).

One should specially mention the scaling of the typical fidelity susceptibility $\chi_F^{(\text{typ})}$ with the system size N. The susceptibility is power-law divergent with N in the multifractal ($1 < \gamma < 2$) and in the mildly localized ($2 < \gamma < 3$) phases, albeit with different exponents $\gamma - 1$ and $3 - \gamma$. However, it vanishes in the limit $N \to \infty$ in the strongly localized phase for $\gamma > 3$, see Figs. 1(b) and 10.

A recent detailed study of an XXZ spin-1/2 chain in a random field [35] revealed a picture (see Fig. 1 therein) which is qualitatively similar to our Figs. 1(b) and 10. For small disorder, the typical fidelity susceptibility is almost size independent and slowly varying with increasing disorder. For intermediate disorder, it gets enhanced (blowing up with increasing the system size), reaches a peak, and then falls down at larger disorder. In the latter region, there is an apparent fixed point W^* in the disorder strength W (similar to $\gamma^* = 3$ in our model) such that with increasing the system size the fidelity susceptibility grows at $W < W^*$ and decreases at $W > W^*$.

We present a qualitative picture explaining the two drastically different regimes of N dependence of the typical fidelity susceptibility both in the Rosenzweig-Porter model with long-range hopping and in short-range hopping models (including interacting systems with two-body interaction corresponding to short-range hopping in the Hilbert space). In the Rosenzweig-Porter model, such a behavior is due to

the nonexponential localization of typical eigenstates, while in short-range systems it is due to the competition between typical exponentially localized states and rare Mott's pairs of states [36–38] emerging as the result of hybridization of two resonant exponentially localized states.

III. THE MODEL AND ITS MAIN PROPERTIES

The Rosenzweig-Porter model [24] is a generalization of the WD random matrix model to the case when diagonal and off-diagonal elements fluctuate with different strengths. Several types of the Rosenzweig-Porter ensembles with various distribution functions of off-diagonal matrix elements have been considered: Gaussian [23], logarithmically- normal [27], and power-law (Levy) [39].

In the simplest GRP model, the Hamiltonian is an $N \times N$ Hermitian real symmetric (orthogonal ensemble, $\beta = 1$) or complex (unitary ensemble, $\beta = 2$) random matrix. Its entries are independent Gaussian-distributed random variables with zero mean and variances ($m \neq n$):

$$\langle H_{nn}^2 \rangle = W^2, \qquad \langle |H_{nm}|^2 \rangle = \sigma^2. \qquad (8)$$

Parameters W and σ, together with the matrix size N, completely specify the GRP model. In the limit of vanishing W, it is equivalent to the usual RMT, with all the states perfectly mixed (ergodic regime) and the average DoS given by the Wigner semicircle with the bandwidth $E_{\text{BW}}^{\text{RMT}} = 2\sqrt{N}\sigma$. In the limit of vanishing σ, we have a perfect localization at each site and the DoS follows the distribution of H_{nn} with the dispersion W.

Remarkably, in the GRP model, the transition from the ergodic to the localized regime goes through an intermediate NEE phase with a fractal statistics of eigenvectors [23]. With increasing W, the crossover from the RMT to the NEE regimes takes place at $W \sim E_{\text{BW}}^{\text{RMT}}$. At larger W, the off-diagonal disorder is too weak to mix all the states and only a part of them, $M \sim (\Gamma/W)N \sim \Gamma/\delta$, participates in the formation of new states from the localized orbitals. Here Γ is the width of the miniband given by (energy close to the band center implied)

$$\Gamma^{\text{NEE}} = \sqrt{2\pi} \frac{N\sigma^2}{W} = 2\pi \frac{\sigma^2}{\delta}. \qquad (9)$$

As W increases, the number M of occupied sites in a typical eigenvector decreases and becomes of the order of 1 when $\Gamma \sim \delta$, where $\delta \sim W/N$ is the mean-level spacing. This point marks the localization transition.

The relevant energy scales discussed above in the ergodic, fractal, and localized regimes are summarized in Table I. Note that in the localized phase, the miniband collapses to a single level, so formally the miniband width is zero. Yet the parameter Γ in the numerator of Eq. (34) remains finite, $\Gamma \sim \sigma \ll \delta$, but apparently loses the meaning of the miniband width [32].

To study the GRP model in the thermodynamic limit, $N \to \infty$, it was suggested in Ref. [23] to use the following scaling of off-diagonal matrix elements:

$$\sigma^2 \propto N^{-\gamma}, \qquad (10)$$

while keeping W independent of the matrix size N. Notice that so-defined γ plays a role of the *effective disorder*

TABLE I. The principal characteristics of the Gaussian RP model in the three phases: the bandwidth E_{BW}, the mean-level spacing δ, and the width Γ of the Lorentzian in Eq. (34) (the latter in the fractal phase has the meaning of the miniband width). Both δ and Γ are calculated at the band center.

Phase	Ergodic	Fractal	Localized
	$\gamma < 1$	$1 < \gamma < 2$	$2 < \gamma$
Condition	$W/\sigma \ll \sqrt{N}$	$\sqrt{N} \ll W/\sigma \ll N$	$N \ll W/\sigma$
E_{BW}	$2\sqrt{N}\sigma$	$\sim W$	$\sim W$
δ	$\sim \sigma/\sqrt{N}$	$\sqrt{2\pi}W/N$	$\sqrt{2\pi}W/N$
Γ	$\sim \sqrt{N}\sigma$	$\sqrt{2\pi}N\sigma^2/W$	$\sim \sigma$

parameter determining the ratio $W^2/(N\sigma^2) \propto N^{\gamma-1}$ of the disorder potential to the kinetic bandwidth.

In the thermodynamic limit, the crossovers between the phases discussed above at a finite N turn into sharp phase transitions at $\gamma = 1$ and $\gamma = 2$, with the ergodic, fractal, and localized phases corresponding to $\gamma < 1$, $1 < \gamma < 2$, and $2 < \gamma$, respectively (see Table I). The miniband width obeys the following scaling [32]:

$$\Gamma \propto \begin{cases} N^{(1-\gamma)/2}, & \text{ergodic}; \\ N^{1-\gamma}, & \text{fractal}. \end{cases} \qquad (11)$$

In terms of the eigenvector statistics, the ergodic phase ($\gamma < 1$) corresponds to the uniform spread of the eigenfunction over all sites, while in the localized phase ($\gamma > 2$) the eigenfunction is highly peaked on a single site. In the intermediate NEE phase ($1 < \gamma < 2$), the eigenvector is fractal with an extensive number of occupied sites which, however, constitutes a vanishing fraction of all available sites. This fractal behavior can be characterized with the help of the eigenvector support set defined as a set of sites r, which is sufficient for the normalization condition $\sum_{r \in \text{SS}} |\Psi_n(r)|^2 = 1 - \epsilon$ to be fulfilled with any prescribed accuracy $\epsilon \ll 1$. The volume of the support set in the fractal phase scales with the matrix size as $M \sim N^D$, with the fractal dimension [23],

$$D = 2 - \gamma, \qquad (12)$$

restricted by $0 < D < 1$. The sites from the support set are nearly resonant and form a compact *miniband* of levels in the energy space of the width $\Gamma \propto N^{D-1}$ [see Eq. (11)] that vanishes in the limit $N \to \infty$ (see Fig. 1). The eigenfunction amplitude statistics in the ergodic phase ($\gamma < 1$) follows the Porter-Thomas distribution $P_{\text{PT}}(x) \propto x^{(\beta-2)/2} \exp(-cx^2)$, like in the classical RMT [1]. The same remains true in the NEE phase as well, provided one restricts $\Psi_n(r)$ to the support set [40].

In general, the amplitude of an eigenvector $|\Psi_n(r)|^2 = |\langle r|n \rangle|^2$ in the GRP model is well approximated by the *Monthus surmise* introduced in Ref. [41]:

$$|\Psi_n(r)|^2 = \frac{|H_{nr}|^2}{(E_n - d_r)^2 + (\Gamma/2)^2}. \qquad (13)$$

Here H_{nr} is the off-diagonal matrix element, $d_r = H_{rr}$ is the diagonal matrix element, and E_n is an exact eigenvalue. In the ergodic phase and in the NEE phase at the support set, the first term in the denominator of the Lorentzian in Eq. (13)
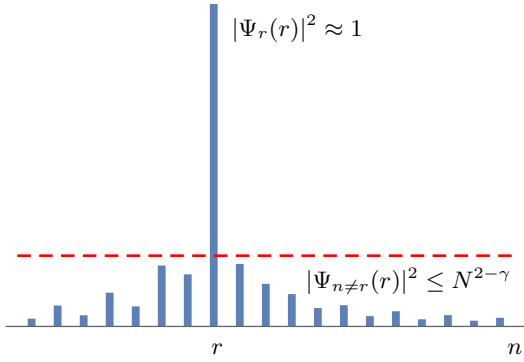
FIG. 3. A typical localized state in the GRP model. In the thermodynamic limit ($N \to \infty$), the localization radius is strictly zero.

can be neglected, and one readily recovers the Porter-Thomas distribution.

The Monthus surmise [Eq. (13)] can also be made meaningful in the localized phase ($\gamma > 2$) if one identifies $\Gamma/2 = \langle|H_{nm}|^2\rangle^{1/2} \sim N^{-\gamma/2}$ [32]. In this case, a wave function $\Psi_n(r)$ is strongly peaked at $n = r$ (see Fig. 3), $E_n \approx d_n$, and Eq. (13) gives $|\Psi_n(r)|^2 \sim \sigma^2/(d_n - d_r)^2$ unless d_n and d_r are in resonance with the accuracy of σ. Since the difference $d_n - d_r$ is typically larger than δ, the amplitude of the wave function $\Psi_{n \neq r}(r)$ is typically bounded from above by

$$|\Psi_{n \neq r}(r)|^2 \lesssim \sigma^2/\delta^2 \propto N^{2-\gamma}. \qquad (14)$$

In fact, for the majority of sites with $|d_n - d_r| \sim E_{\mathrm{BW}} \propto N^0$, the wave function is much smaller: $|\Psi_n(r)|^2 \sim \sigma^2/W^2 \propto N^{-\gamma}$. The contribution of $n \neq r$ sites to the normalization integral can be estimated as $\sum_{n \neq r} |\Psi_n(r)|^2 \sim \sum_{n \neq r} \sigma^2/\delta^2(n - r)^2 \sim \sigma^2/\delta^2 \propto N^{2-\gamma}$ due to fast convergence of the sum, which effectively saturates by a finite number of levels n adjacent to r. Hence,

$$1 - |\Psi_r(r)|^2 \sim \sigma^2/\delta^2 \propto N^{2-\gamma}, \qquad (15)$$

and in the thermodynamic limit ($N \to \infty$) $\langle r|n\rangle = \delta_{nr}$, i.e., an eigenvector is localized strictly on a single site at *any* $\gamma > 2$, as shown in Fig. 3.

An important extension of the GRP is the LN-RP ensemble with the *tailed* distribution of off-diagonal matrix elements $P(|H_{nm}|)$:

$$P(x) = \frac{A}{x} \exp\left[-\frac{\ln^2(x/x_{\mathrm{typ}})}{2p \ln(1/x_{\mathrm{typ}})}\right]. \qquad (16)$$

The LN-RP ensemble is specified by two parameters: γ and p. The former determines the *typical* value of the off-diagonal matrix element:

$$H^{(\mathrm{typ})} \equiv \exp\langle\ln|H_{nm}|\rangle \sim N^{-\gamma/2}. \qquad (17)$$

The parameter p controls the strength of the *tail* in the distribution function Eq. (16), which becomes thicker as p increases. In the limit $p \to 0$, the LN-RP model approaches the GRP, while the special choice $p = 1$ brings the model in the same universality class as the Anderson model on RRG [11]. Remarkably, for $p > 0$ the LN-RP model possesses a nontrivial dynamics. For instance, the ensemble-averaged *survival probability* in some parameter region decays with time

as a *stretch exponent* [11], in contrast to a simple exponential decay in the delocalized phases of GRP.

One can also consider [39] the Levy-RP model with a power-law distribution $P(x) = A/x^{1+k}$ (the parameter $k > 0$) truncated at $|x| < x_{\mathrm{typ}}$, which is in many respects similar to LN-RP model.

IV. FIDELITY SUSCEPTIBILITY χ_{F} AND EIGENSTATE AMPLITUDE OVERLAP CORRELATION FUNCTION $K(\omega)$

A. General expression for χ_{F}

The fidelity of two states $|n(0)\rangle$ and $|n(\lambda)\rangle$ belonging to the Hamiltonians $\widehat{H}(0)$ and $\widehat{H}(\lambda)$ is defined as

$$F_n^2(\lambda) = |\langle n(0)|n(\lambda)\rangle|^2. \qquad (18)$$

Since the set of eigenstates $|m\rangle = |m(0)\rangle$ is complete and orthonormal, one can write

$$F_n^2(\lambda) = 1 - \sum_{m \neq n} |\langle m|n(\lambda)\rangle|^2. \qquad (19)$$

To express the fidelity behavior at $\lambda \to 0$ in terms of the eigensystem of the Hamiltonian $\widehat{H}(0)$, we employ the Hellmann-Feynman relation,

$$\langle m|\partial_\lambda n\rangle = \frac{\langle m|\partial_\lambda \widehat{H}|n\rangle}{E_n - E_m}, \qquad (20)$$

which can be derived by differentiating the Schrödinger equation $\widehat{H}(\lambda)|n(\lambda)\rangle = E_n(\lambda)|n(\lambda)\rangle$ with respect to the parameter λ. The fidelity susceptibility defined by Eq. (6) is then given by [33–35]

$$\chi_{\mathrm{F}}^{(n)} \equiv -\frac{dF_n^2}{d\lambda^2}\bigg|_{\lambda=0} = \sum_{m \neq n} \frac{|\langle m|\partial_\lambda \widehat{H}|n\rangle|^2}{(E_m - E_n)^2}\bigg|_{\lambda=0}. \qquad (21)$$

Equation (21) is general and applies to any system.

Due to the denominator $(E_m - E_n)^2$ in Eq. (21), the fidelity susceptibility $\chi_{\mathrm{F}}^{(n)}$ is a random and strongly fluctuating function of state n. To get rid of this irregularity, one can also define a fidelity susceptibility averaged over the spectrum *in any given realization* of disorder:

$$\chi_{\mathrm{F}} = \frac{1}{N}\sum_n \chi_{\mathrm{F}}^{(n)} = \frac{1}{N}\sum_n \sum_{m \neq n} \frac{|\langle m|\partial_\lambda \widehat{H}|n\rangle|^2}{(E_m - E_n)^2}\bigg|_{\lambda=0}. \qquad (22)$$

In what follows, we will study this *spectral-averaged* fidelity susceptibility.

B. Fidelity susceptibility for a local density drive

For further applications, we choose a specific perturbation $\partial_\lambda \widehat{H}$ proportional to the *local density* operator:

$$\partial_\lambda \widehat{H} = N\delta\, |r\rangle\langle r|. \qquad (23)$$

Then the matrix element in Eq. (21) becomes a product of two wave functions at the given point r:

$$\langle m|\partial_\lambda \widehat{H}|n\rangle = N\delta\, \langle m|r\rangle\, \langle r|n\rangle \equiv N\delta\, \Psi_m^{(0)}(r)\Psi_n^{(0)*}(r). \qquad (24)$$

As a result, the spectral-averaged fidelity susceptibility acquires the form

$$\chi_{\mathrm{F}} = 2\delta \int_0^\infty \frac{\mathfrak{C}(\omega, r)}{\omega^2} \, d\omega, \qquad (25)$$

where

$$\mathfrak{C}(\omega, r) = N\delta \sum_n \sum_{m \neq n} \rho_n^{(0)}(r) \rho_m^{(0)}(r) \delta(\omega - \omega_{mn}) \qquad (26)$$

and $\omega_{nm} = E_n^{(0)} - E_m^{(0)}$. Note that the *ensemble-averaged* value of $\mathfrak{C}(\omega, r)$ can be expressed in terms of $C_E(\omega, \lambda)$ defined in Eq. (3):

$$\langle \mathfrak{C}(\omega, r) \rangle = \int \frac{dE}{N\delta} C_E(\omega, \lambda = 0) \sim C(\omega, 0). \qquad (27)$$

Since $C_E(\omega, \lambda = 0)$ is weakly E dependent inside the spectral bandwidth $|E| \lesssim N\delta$ and is almost zero beyond it, the integral in Eq. (27) is equal to $C(\omega, 0) \equiv C_0(\omega, 0)$ up to a prefactor of order 1.

The fidelity susceptibility given by Eq. (25) is a random quantity with some distribution function $P(\chi_{\mathrm{F}})$. An important feature of this distribution is the presence of a power-law tail at large χ_{F}, originating from the factor ω^2 in the denominator of Eq. (25). Indeed, in this regime the sum in Eq. (22) is dominated by a single term with the smallest $\omega_{nm} = |E_n - E_m| \ll \delta$, and $P(\chi_{\mathrm{F}})$ is determined by the strength of level repulsion. With $\mathfrak{C}(\omega, r) \sim \omega^\beta$, we obtain the large-$\chi_{\mathrm{F}}$ asymptotics: $P(\chi_{\mathrm{F}}) \sim \chi_{\mathrm{F}}^{-(3+\beta)/2}$. This power-law tail causes the divergence of the *ensemble-averaged* fidelity susceptibility in the localized phase ($\beta = 0$) and in the extended phase for the orthogonal symmetry class ($\beta = 1$) (the extended phase of the unitary symmetry with $\beta = 2$ is characterized by a finite $\langle \chi_{\mathrm{F}} \rangle$).

The maximum of the distribution function $P(\chi_{\mathrm{F}})$ is reached when *many* terms start to be relevant in the sum in Eq. (21). Thus, the *typical* value $\chi_{\mathrm{F}}^{(\mathrm{typ})}$ of χ_{F}, characterized by the maximal probability, corresponds to the smallest $|E_n - E_m|$ being of the order of the typical level spacing (that for RP models coincides with the mean-level spacing δ). This suggests that the typical fidelity susceptibility is given by

$$\chi_{\mathrm{F}}^{(\mathrm{typ})} \sim \delta \int_\delta^\infty C^{(\mathrm{typ})}(\omega, 0) \frac{d\omega}{\omega^2}, \qquad (28)$$

where $C^{(\mathrm{typ})}(\omega, 0)$ is the typical value of $\mathfrak{C}(\omega, r)$:

$$C^{(\mathrm{typ})}(\omega, \lambda = 0) = \exp\langle \ln \mathfrak{C}(\omega, r) \rangle. \qquad (29)$$

Taking into account that for $\omega > \delta$ the DoS correlation function $R^{(\mathrm{typ})}(\omega, 0) = R(\omega, 0) \approx 1$ [where $R^{(\mathrm{typ})}(\omega, 0)$ corresponds to the typical DoS correlation function similar to Eq. (29)], one may rewrite Eq. (28) as

$$\chi_{\mathrm{F}}^{(\mathrm{typ})} \sim \delta \int_\delta^\infty K^{(\mathrm{typ})}(\omega, 0) \frac{d\omega}{\omega^2}. \qquad (30)$$

Now, given that the integral in Eq. (30) is dominated by the lower limit, we arrive at

$$\chi_{\mathrm{F}}^{(\mathrm{typ})} \sim K^{(\mathrm{typ})}(\delta, 0). \qquad (31)$$

Equation (31) applies to a generic case when $K^{(\mathrm{typ})}(\omega, \lambda)$ does not coincide with $K(\omega, \lambda)$, e.g., to the LN-RP model and for models with short-range hopping. For the Gaussian RP model with the tail-free distribution of off-diagonal matrix elements, $K^{(\mathrm{typ})}(\omega, \lambda)$ coincides with $K(\omega, \lambda)$, and Eq. (31) leads to the estimate (7).

C. Parametric density correlation function at a diagonal drive within the Monthus surmise approximation

In this subsection, we make a simple derivation of the parametric density correlation function $\tilde{K}(\omega, \lambda)$ [Eq. (5)] based on the Monthus surmise approximation, Eq. (13). An exact derivation in Sec. V based on the supersymmetric NLSM confirms the validity of this simple derivation in the fractal phase at the energy scale $|\omega + \lambda W| \gg \delta$, when level repulsion effects can be neglected.

In both derivations, we assume the diagonal drive:

$$\widehat{H}_2 = \widehat{d'} = \mathrm{diag}\{d_n'\}. \qquad (32)$$

Let us first consider the *fractal* phase with the hierarchy of scales $\delta \ll \Gamma \ll E_{\mathrm{BW}}$, see Table I. Substituting Eq. (13) into Eq. (5), we can express $\tilde{K}(\omega, \lambda)$ in terms of the eigenfunction overlap at $E_n - E_m = \omega$,

$$\tilde{K}(\omega, \lambda) = \frac{4\pi^2 N^2}{\Gamma^2} \big\langle |H_{nr}|^2 |H_{mr}|^2 \mathcal{L}(d_r - \tilde{\omega}) \mathcal{L}(d_r) \big\rangle, \qquad (33)$$

where $\mathcal{L}(\omega) = (\Gamma/2\pi)[\omega^2 + (\Gamma/2)^2]^{-1}$ is a normalized Lorentzian.

Equation (33) should be averaged over the matrix elements H_{nr}, H_{mr}, and $H_{rr} = d_r$ of the Hamiltonian $\widehat{H}_1$, and over the diagonal matrix elements d_r' of $\widehat{H}_2$ (which determine the shifted frequency $\tilde{\omega} = \omega - \lambda d_r'$); all of them are independently fluctuating. The averaging over off-diagonal matrix elements gives σ^4, while the averaging over d_r is Gaussian with the variance W^2 [Eqs. (8)]. Then using the fact that the convolution of two Lorentzians is a Lorentzian of the double width and relying on the relations of Table I, one obtains

$$\tilde{K}(\omega, \lambda) = \frac{1}{\pi} \frac{N}{M} \left\langle \frac{\Gamma^2}{(\omega - \lambda d_n')^2 + \Gamma^2} \right\rangle_{d_n'}, \qquad (34)$$

where $\langle \ldots \rangle_{d_n'}$ denotes the averaging over the diagonal matrix element d_n' of the Hamiltonian $\widehat{H}_2$, and $M = \Gamma/\delta$ is the number of states in the miniband. Note that the diagonal drive $\widehat{d'}$ in Eq. (34) should not necessarily be Gaussian.

Equation (34) remains valid in the *localized* phase characterized by $M = 1$ and $\Gamma \sim \sigma \ll \delta$ (see Table I). Since the Monthus surmise is based on the Wigner-Weisskopf approximation [42] and the latter is valid only for times shorter than the Heisenberg time $t_{\mathrm{H}} = \hbar/\delta$, Eq. (34) is justified only for $|\tilde{\omega} - \lambda d_n'| \gg \delta$. Therefore, in the localized phase with $\sigma \ll \delta$ the relaxation rate Γ in the *denominator* of Eq. (34) is not well defined and should be neglected. Then, Eq. (34) acquires a perfectly perturbative form

$$\tilde{K}(\omega, \lambda) \propto \frac{\sigma^2}{(\omega - \lambda d_n')^2} \quad \text{for } |\omega - \lambda d_n'| \gg \delta, \qquad (35)$$

as it should be with σ being the smallest parameter of the problem.

By the order of magnitude, Eq. (34) remains valid also in the *ergodic* phase when $M \sim N$, $\Gamma \sim E_{\mathrm{BW}} \to \infty$ and,
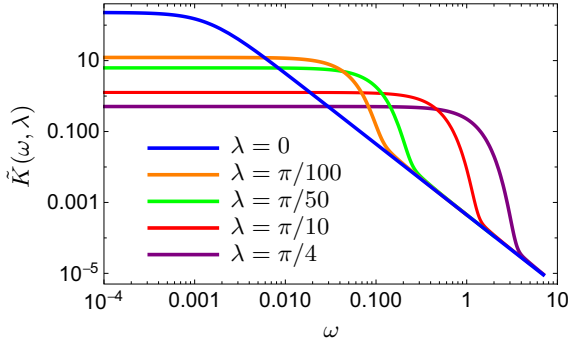
FIG. 4. Density correlation function $\tilde{K}(\omega, \lambda)$ [Eq. (34)] for $\Gamma = 0.0014$ and Gaussian distribution of d'_n with the variance $W^2 = 1/2\pi$ at various values of the control parameter λ.

consequently, $\tilde{K}(\omega, \lambda) \sim 1$. For the Gaussian distribution of d'_n, the density correlation function given by Eq. (34) is plotted in Fig. 4.

Vice versa, if the density correlation function $\tilde{K}(\omega, \lambda)$ is known, then using Eq. (34) one can extract the effective distribution function $\mathcal{P}_\lambda(\Delta)$ of the random shift $\Delta = \lambda d'_n$ from the following relation:

$$\mathcal{P}_\lambda(\Delta) = \int \frac{dt}{2\pi} \frac{G(t, \lambda)}{G(t, 0)} e^{it\Delta}, \tag{36}$$

where $G(t, \lambda)$ is the Fourier transform of $K(\omega, \lambda)$.

Equation (36) is strictly derived under an assumption of the Lorentzian-like form of the density correlator (34). Nevertheless, we will use it as an operational definition of $\mathcal{P}_\lambda(\Delta)$ in a generic situation.

D. $\chi_F^{(typ)}$ and its scaling in different phases

Here, based on Eqs. (7), (34), and (35), we discuss the fidelity susceptibility and its scaling in the limit $N \to \infty$. Summarizing the results of Sec. IV C for $\tilde{K}(\delta, 0)$, plugging them into Eq. (7), and using relations of Table I, we obtain

$$\chi_F^{(typ)} \sim \begin{cases} 1 \propto N^0, & \gamma < 1 \\ N\delta/\Gamma \propto N^{\gamma-1}, & 1 < \gamma < 2 \\ N(\sigma/\delta)^2 \propto N^{3-\gamma}, & 2 < \gamma. \end{cases} \tag{37}$$

To illustrate the validity of Eq. (7) in the localized phase, one may substitute Eq. (24) into Eq. (22) and note that the main contribution comes from $m = r$ (the choice $n = r$ doubles the result) when $\Psi_r(r) \approx 1$. Then, using the Monthus surmise (13) for $\Psi_n(r)$, one obtains

$$\chi_F = 2N\delta^2 \sum_{n \neq r} \frac{|H_{nr}|^2}{(E_r - E_n)^4}. \tag{38}$$

For the tail-free Gaussian distribution of H_{nr}, the typical value of the fidelity susceptibility, $\chi_F^{(typ)}$, corresponds to the typical minimal distance $|E_r - E_n| \sim \delta \sim W/N$, while $|H_{nr}|^2$ can be replaced by its average σ^2. Thus, we readily reproduce the last line in Eq. (37), confirming the validity of Eq. (7) in this particular case.

Taking the derivative of $\ln \chi_F^{(typ)}$ with respect to $\ln N$ eliminates N-independent prefactors in Eq. (37), leading to the

following asymptotically exact scaling:

$$\frac{d \ln \chi_F^{(typ)}}{d \ln N} = \begin{cases} 0, & \gamma < 1 \\ \gamma - 1, & 1 < \gamma < 2 \\ 3 - \gamma, & 2 < \gamma. \end{cases} \tag{39}$$

This result is shown by the red dashed line in Fig. 1(b).

Note that the derivative $d \ln \chi_F^{(typ)}/d \ln N$ changes sign at a fixed point $\gamma^* = 3$ which lies *inside* the localized phase. This result can be traced back to the behavior of the eigenfunction amplitude, Eq. (14). Indeed, since for the GRP model $K(\omega, \lambda) \approx \tilde{K}(\omega, \lambda)$, both being independent of r, it follows from Eq. (5) that

$$K(\delta, 0) \approx N \sum_r \langle |\Psi_m(r)|^2 |\Psi_{m+1}(r)|^2 \rangle. \tag{40}$$

The leading contribution to Eq. (40) comes either from $r = m$ [where $\Psi_r(r) \approx 1$] or from $r = m + 1$. Then, Eqs. (7) and (14) provide an estimate:

$$\chi_F^{(typ)} \sim N\sigma^2/\delta^2 \propto N^{3-\gamma}. \tag{41}$$

Thus the change of sign of the logarithmic derivative $d \ln \chi_F^{(typ)}/d \ln N$ happens when the amplitude $|\Psi|^2$ of one state at a site where the adjacent in energy state is localized is of the order of $1/N$. In other words, at the fixed point $\gamma = \gamma^*$ the maximal overlap

$$J_{nm} = W \sum_r |\Psi_n(r)|^2 |\Psi_m(r)|^2 \tag{42}$$

between two different *typical* localized states becomes of the order of δ,

$$\max_m \{J_{n \neq m}\}\big|_{\gamma = \gamma^*} \sim \delta, \tag{43}$$

with $\max_m\{J_{n \neq m}\} \gg \delta$ for $\gamma < \gamma^*$ (weaker disorder) and $\max_m\{J_{n \neq m}\} \ll \delta$ for $\gamma > \gamma^*$ (stronger disorder).

E. Generalization to short-range hopping models: The role of resonant Mott's pairs

The condition (43) for the critical disorder strength where $d \ln \chi_F^{(typ)}/d \ln N$ changes its sign was derived for the GRP model characterized by an infinite-range hopping. In fact, it is much more general and applies also to systems with *short-range* hopping, such as the Anderson model on d-dimensional lattices and graphs. However, in that case the meaning of $\max\{\cdot\}$ needs to be specified.

Indeed, a typical localized state in such systems has a single localization center ("head"), with $|\Psi_n(r)|^2$ decreasing exponentially as r is shifting away from this center. Therefore, two such states with a distance R_{nm} between their heads have an exponentially small overlap $J_{nm} \sim W \exp(-R_{nm}/\xi)$, where ξ is the localization radius. Since the typical distance between the localization centers R_{nm} is of the order of the system size L, such single-headed states make an *exponentially small* contribution to $K(\delta, 0)$ and hence to the fidelity susceptibility that would *decrease* with increasing L. This statement is true provided that only typical states are considered.

On the other hand, it is known [36–38] that two *resonant* localized single-headed states $\Psi_n(r)$ and $\Psi_m(r)$ may effectively hybridize to form a Mott's pair of bonding and

antibonding states, $\Psi_\pm(r) = [\Psi_n(r) \pm \Psi_m(r)]/\sqrt{2}$. The resulting double-headed states have the level splitting $\Delta E \sim J_{nm}$ given by the overlap of the parent states $\Psi_n(r)$ and $\Psi_m(r)$. The distance $R_{nm} = R_{\Delta E}$ between the heads of the parent states required to form a Mott's pair grows with decreasing ΔE as $R_{\Delta E} \sim \xi \ln(W/\Delta E)$. Though such pairs of double-headed states are rare, their overlap,

$$J_{nm} \approx \frac{W}{4} \sum_r \left\{ |\Psi_n(r)|^4 + |\Psi_m(r)|^4 \right\}, \qquad (44)$$

is independent of the system size. Thus the formation of Mott's pairs results in an *exponentially large* gain in the overlap compared to that of the parent states.

This gain makes the Mott's pairs a serious competitor to single-headed states for the leading contribution to $K(\delta, 0)$, with the winner depending on the particular type of average considered. Mott's pairs contribution determines the *far tail* of the distribution of random overlaps J_{nm} which dominates in the *mean* $K(\delta, 0)$. However, typical states are single-headed. Therefore taking the *typical average* $K^{(\text{typ})}(\delta, 0)$ [as in Eq. (30)], one cuts the tail of the distribution and strongly discriminates the contribution of Mott's pairs. As a result, at strong enough disorder (analogous to our $\gamma > \gamma^*$), the *typical* $K^{(\text{typ})}(\delta, 0) \sim \chi_F^{(\text{typ})}$ *decreases* exponentially with the system size, in contrast to the *mean* $K(\delta, 0)$ which always (except for the case of one-dimensional single-particle localization) *increases* with L. The reason for such an anomalous behavior is the dominance of Mott's pair contribution in the mean $K(\delta, 0)$.

Indeed, it is known that if only the Mott's pair contribution is taken into account, the averaged $K(\omega, 0)$ would increase with decreasing $\omega \gtrsim \delta$ [12,31] and hence $K(\delta, 0)$ would increase with increasing the system size L. Notice that only the pairs with the level splitting $\Delta E = \delta$ make a contribution to this quantity. Notice also that $R_{\Delta E=\delta} \propto \ln(W/\delta) \sim \ln N$ is growing with increasing the system size. Since the probability of forming a resonant Mott's pair of states is proportional to the area $S = S(\Delta E)$ of a sphere of radius $R = R_{\Delta E}$ in a d-dimensional ($S \sim R^{d-1}$) or in an ultrametric ($S \sim \mathcal{K}^R$) space, this probability for $\Delta E = \delta \sim 1/N$ is increasing with the system size. As the overlap J_{nm} for a Mott's pair is independent of the system size, the increase of probability to find a Mott's pair leads to an increase of the averaged $K(\delta, 0)$.

Summarizing, we can say that if the Mott's pair contribution is dominant in $K^{(\text{typ})}(\delta, 0) \sim \chi_F^{(\text{typ})}$, the typical fidelity susceptibility grows with the system size, otherwise it decreases with it.

The condition for the boundary between the two regimes can be formulated in a form of Eq. (43), with the left-hand side determined by the competition between double-headed and single-headed states. Since the probability to find a resonant Mott's pair decreases with increasing the level splitting ΔE, there should be a maximal ΔE for which the contribution of the Mott's pairs to the typical $K^{(\text{typ})}(\delta, 0)$ still dominates over that of typical single-headed states. A particular value of ΔE is system dependent, and it is the corresponding $\max_m\{J_{n\neq m}\} \sim \max\{\Delta E\}$ that enters the criterion (43) in the case of the short-range hopping systems.

The peculiarity of the GRP model is that in this case the localization is *not exponential*, contrary to models with short-range hopping. Therefore, even *typical* single-headed states may lead to both increasing and decreasing with the systems size *mean* $K(\delta, 0)$ [which in the GRP model is of the same order as $K^{(\text{typ})}(\delta, 0) \sim \chi_F^{(\text{typ})}$]. Another important difference is that in GRP the transition between the two regimes of diverging and vanishing fidelity susceptibility is a sharp phase transition in the limit $N \to \infty$ rather than a crossover, as in systems with short-range hopping.

V. ANALYTICAL RESULTS FOR PARAMETRIC CORRELATION FUNCTIONS IN THE CASE OF DIAGONAL DRIVE

A. General expressions in the fractal phase

In this section, we review analytical results for the DoS, LDoS, and EAO parametric correlation functions obtained in the framework of the supersymmetric NLSM for the *unitary* GRP model in its *fractal phase* subject to the *diagonal drive*. The validity of the NLSM is justified by the large ratio $g = E_{\text{Th}}/\delta$ of the Thouless energy E_{Th} to the mean-level spacing that allows us to neglect the longitudinal models and enforce the sigma-model constraint $Q^2 = 1$. In the fractal phase, the Thouless energy is given by $E_{\text{Th}} = \sqrt{\Gamma\delta}$ [32] and hence $g = \sqrt{\Gamma/\delta} \gg 1$, justifying the NLSM approach in the whole fractal phase where $\Gamma \gg \delta$ (see Table I). Adopting the scaling Eq. (10), one obtains $g \propto N^{1-\gamma/2} \to \infty$ as long as $1 < \gamma < 2$.

The results we present below correspond to the limit $N \to \infty$ and apply to the fractal phase ($\Gamma \gg \delta$). They are calculated at the band center ($E \ll E_{\text{BW}}$ and $\omega \ll E_{\text{BW}}$) and are valid for an arbitrary value of ω/δ. The general expressions for $R(\omega, \lambda)$ and

$$C(\omega, \lambda) = \frac{N\delta}{\pi\Gamma} \bar{C}(\omega, \gamma), \qquad (45)$$

as they emerge from the formalism of the NLSM, read

$$R(\omega, \lambda) = 1 + \frac{1}{2} \text{Re} \int_{-1}^{1} d\lambda_{\text{F}} \int_{1}^{\infty} d\lambda_{\text{B}} \, P_R \, e^S + \frac{C(\omega, \lambda)}{N}, \quad (46)$$

$$\bar{C}(\omega, \lambda) = \left\langle \frac{\Gamma^2}{\tilde{\omega}^2 + \Gamma^2} \right\rangle_{d'} + \text{Re} \int_{-1}^{1} d\lambda_{\text{F}} \int_{1}^{\infty} d\lambda_{\text{B}} \, \frac{P_C \, e^S}{\lambda_{\text{B}} - \lambda_{\text{F}}}, \qquad (47)$$

where integration is performed over two Cartan variables λ_{F} and λ_{B} specific to the unitary (class A) symmetry, the action is given by

$$S = \frac{i\pi}{\delta}(\lambda_{\text{B}} - \lambda_{\text{F}}) \left\langle \frac{\Gamma\tilde{\omega}}{\tilde{M}_B^{1/2}} \right\rangle_{d'}, \qquad (48)$$

and the functions $P_R(\lambda_{\text{B}})$ and $P_C(\lambda_{\text{B}})$ are defined as

$$P_R = \left\langle \frac{\Gamma^2(\Gamma - i\tilde{\omega}\lambda_{\text{B}})}{\tilde{M}_B^{3/2}} \right\rangle_{d'}^2, \qquad (49)$$

$$P_C = \left\langle \frac{2\tilde{M}_B\lambda_{\text{B}} + 3i\Gamma\tilde{\omega}(\lambda_{\text{B}}^2 - 1)}{2\tilde{M}_B^{5/2}/\Gamma^3} \right\rangle_{d'}. \qquad (50)$$

In these expressions,

$$\tilde{M}_B = \Gamma^2 - \tilde{\omega}^2 - 2i\Gamma\tilde{\omega}\lambda_{\text{B}}, \qquad (51)$$

with $\tilde{\omega} = \omega - \lambda d'$ being a λ-dependent random quantity, and the symbol $\langle \ldots \rangle_{d'}$ stands for averaging over the distribution of the diagonal matrix element d' of the Hamiltonian $\widehat{H}_2$. The expressions provided above refine Eq. (34) at a scale of $\tilde{\omega}$ of the order of or less than the mean-level spacing δ.

Remarkably, the last term of Eq. (46) is exactly equal to $C(\omega, \lambda)/N$. Thus the global DoS correlation function includes the local one, albeit as a $1/N$-effect.

The formal derivation of the results (46) and (47) is given in the Appendix.

B. DoS correlation function $R(\omega, \lambda)$: Smearing of the delta peak

Of special interest is the behavior of $R(\omega, \lambda)$ at small $\omega \ll \Gamma$ since it gives a response of individual levels to perturbation. To obtain an approximate expression in this limit, one can neglect the last term in Eq. (46) and assume $P_R = 1$. Then, expanding $\tilde{M}_B^{-1/2}$ in the action and keeping the leading terms in ω/Γ and $\lambda d'$, one obtains after the averaging over d':

$$R(\omega, \lambda) = 1 + \tfrac{1}{2} \operatorname{Re} F(x, \alpha), \qquad (52)$$

where

$$F(x, \alpha) = \int_{-1}^{1} d\lambda_{\mathrm{F}} \int_{1}^{\infty} d\lambda_{\mathrm{F}} \exp[(ix - \alpha\lambda_{\mathrm{B}})(\lambda_{\mathrm{B}} - \lambda_{\mathrm{F}})] \qquad (53)$$

and we introduced two dimensionless parameters:

$$x = \pi\omega/\delta, \qquad (54)$$

$$\alpha = \frac{\pi\lambda^2 \langle d'^2 \rangle}{\Gamma\delta}. \qquad (55)$$

Integration over λ_{F} in Eq. (53) can be easily performed and we arrive at

$$R(\omega, \lambda) = 1 + \operatorname{Re} \int_{1}^{\infty} d\lambda_{\mathrm{B}} \, e^{-(\alpha\lambda_{\mathrm{B}} - ix)\lambda_{\mathrm{B}}} \frac{\sinh(\alpha\lambda_{\mathrm{B}} - ix)}{\alpha\lambda_{\mathrm{B}} - ix}. \qquad (56)$$

The function $R(\omega, \lambda)$ at various values of the control parameter λ is plotted in Fig. 2(a). At $\lambda \to 0$, this function approaches the WD limit (shown by the gray dashed line)

$$R_{\mathrm{WD}}(\omega) = \delta(x) + 1 - (\sin x/x)^2, \qquad (57)$$

characterized by the δ-function peak of the level self-correlation and quadratic level-repulsion $R_{\mathrm{WD}}(\omega) \sim x^2$ at $x \ll 1$. At sufficiently small λ, the self-correlation peak and small-x suppression of $R(\omega, \lambda)$ are still present. However, the peak is progressively broadened and lowered as λ increases and eventually eats up all the correlation hole, making the function $R(\omega, \lambda) \approx 1$ essentially flat, see Fig. 2(a).

C. LDoS correlation function $C(\omega, \lambda)$

Comparing Eq. (34) with Eqs. (45) and (47), we see that $\tilde{K}(\omega, \lambda) = C^{(\mathrm{L})}(\omega, \lambda)$, where $C^{(\mathrm{L})}(\omega, \lambda)$ is the first (Lorentzian) term in the LDoS correlation function. This term describes the random shift of the *entire miniband,* following the shift of a diagonal term in the Hamiltonian, see Fig. 1(a). The coincidence of the two results is an indirect proof of the Monthus surmise, Eq. (13).

At an energy scale $\tilde{\omega} \sim \Gamma$, the second term in Eq. (47) is a correction to the first one. However, at $\tilde{\omega} \lesssim \delta \ll \Gamma$ it becomes

significant, as it describes the shift of *a single level* due to perturbation. In this region, Eq. (47) reduces to

$$\bar{C}(\omega, \lambda) = 1 + \operatorname{Re} \Phi(x, \alpha), \qquad (58)$$

where, similar to Eq. (53),

$$\Phi(x, \alpha) = \int_{-1}^{1} d\lambda_{\mathrm{F}} \int_{1}^{\infty} \frac{\lambda_{\mathrm{B}} d\lambda_{\mathrm{B}}}{\lambda_{\mathrm{B}} - \lambda_{\mathrm{F}}} \exp[(ix - \alpha\lambda_{\mathrm{B}})(\lambda_{\mathrm{B}} - \lambda_{\mathrm{F}})]. \qquad (59)$$

To facilitate the integration in Eq. (59), we first differentiate it with respect to ix and perform integration over λ_{F}. Then, integration over ix can be done using the formula

$$\int e^{-\lambda_{\mathrm{B}}z} \frac{\sinh z}{z} dz = \frac{\operatorname{Ei}[z(1 - \lambda_{\mathrm{F}})] - \operatorname{Ei}[-z(1 + \lambda_{\mathrm{B}})]}{2}, \quad (60)$$

where $z = -ix + \alpha\lambda_{\mathrm{B}}$ and $\operatorname{Ei}(x)$ is the exponential integral function. Finally, one arrives at

$$\bar{C}(\omega, \lambda) = 1 + \operatorname{Re} \int_{1}^{\infty} [I(\lambda_{\mathrm{B}}; x, \alpha) + I(-\lambda_{\mathrm{B}}; -x, \alpha)] \, d\lambda_{\mathrm{B}}, \qquad (61)$$

where

$$I(\lambda_{\mathrm{B}}; x, \alpha) = \lambda_{\mathrm{B}} \operatorname{Ei}[ix - \lambda_{\mathrm{B}}(\alpha - ix) - \alpha\lambda_{\mathrm{B}}^2]. \qquad (62)$$

The function $\bar{C}(\omega, \lambda)$ is plotted in Figs. 2(b) and 2(c). It also shows a broadened self-correlation peak and the correlation hole, the latter being essentially the same in the LDoS correlation function $\bar{C}(\omega, \lambda)$ and in the global DoS correlation function $R(\omega, \lambda)$.

D. EAO correlation function $K(\omega, \lambda)$ at small λ

It is remarkable that in the function $K(\omega, \lambda)$, the level repulsion features cancel out [see the inset in Fig. 2(b)]. That supports the assumption of the statistical independence of the eigenfunction and spectral fluctuations in the GRP model. The function $\bar{K}(\omega, \lambda) - 1 \equiv \bar{C}(\omega, \lambda)/R(\omega, \lambda) - 1$ is strictly positive, albeit vanishing in the limit $\omega \gg \delta$. Thus the effect of *spectral* correlations (the correlation hole due to level repulsion) is absent in $K(\omega, \lambda)$, so it is essentially dominated by the *eigenfunction amplitude correlations* and describes the broadened self-correlation peak. This peak represents a (not normalized) distribution of the shift of a level at a small perturbation. Figure 5 demonstrates that the width of the peak, which gives a typical shift $\Delta E_n = E_n^{(\lambda)} - E_n^{(0)}$ of an individual level, is proportional to $\alpha^{1/2}\delta$ at $\alpha \ll 1$, i.e., it is linear in the perturbation strength λ:

$$\frac{\Delta E_n}{\delta} \sim \alpha^{1/2} \sim \lambda \langle d'^2 \rangle^{1/2} N^{\gamma/2} \quad (1 < \gamma < 2). \qquad (63)$$

VI. NUMERICAL RESULTS

In this section, we present the results of numerical computation of the parametric correlation function $\tilde{K}(\omega, \lambda)$ of the density operators [Eq. (5)]. In practice, two narrow bins were located at energies $E = \varepsilon$ and $E = \varepsilon + \omega$ with ε being close to the band center. In each disorder realization, the sum of the products $\rho_n^{(0)}(r)\rho_m^{(\lambda)}(r) \equiv \rho_1\rho_2$ of those states whose energies $E_n^{(0)}$ and $E_m^{(\lambda)}$ fall in the first and second bins, respectively, was divided by the product of the number of states n_1 and n_2 in each bin and *after that* averaged over GRP ensemble
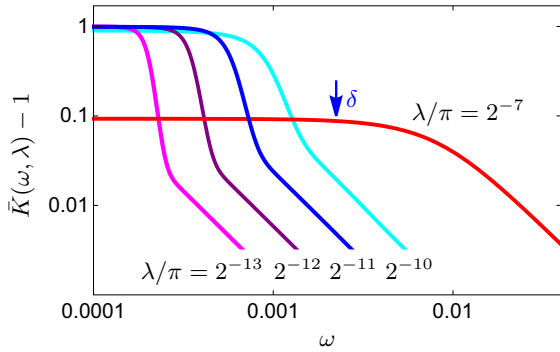
FIG. 5. Broadened self-correlation peak. The function $\bar{K}(\omega, \lambda) - 1 \equiv \bar{C}(\omega, \lambda)/R(\omega, \lambda) - 1$ versus ω for various control parameters $\lambda = \pi/128, \pi/1024, \pi/2048, \pi/4096, \pi/8192$ obtained using Eqs. (56) and (61). The parameters of the GRP model are $N = 1024$ and $\gamma = 3/2$. At a small perturbation $\alpha \ll 1$, it has almost a box-shaped form with a width $\sim \alpha^{1/2}\delta$ and a tail $\propto \omega^{-2}$ (the cyan through magenta curves). At large perturbation $\alpha \gg 1$, the peak approaches a Lorentzian shape (the red curve).
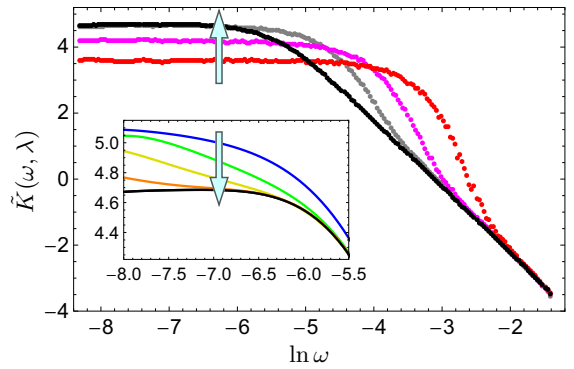

FIG. 6. EAO for the diagonal drive. The function $\tilde{K}(\omega, \lambda)$ from the numerical diagonalization of the Hamiltonian Eq. (1) with a diagonal $\widehat{H}_2$ at $N = 1024$, $W = 1$, $\sigma^2 = 0.1 N^{-\gamma}$, $\gamma = 3/2$ and $\lambda = \pi/512$ (gray), $\pi/256$ (magenta), $\pi/128$ (red), and $\lambda = 0$ (black). The arrows show the direction of evolution as λ is decreasing. Inset: The broadened self-correlation bump in $\tilde{K}(\omega, \lambda)$ at small ω for a weak drive $\lambda = \pi/2048$, (blue) $\lambda = \pi/4096$ (green), $\lambda = \pi/8192$ (yellow), $\lambda = \pi/16384$ (orange). The self-correlation peak makes the direction of evolution opposite to that at a strong drive on the main plot.

realizations. The scan over ε in an energy strip centered at $E = 0$ and containing $1/32$ of all levels was also taken to improve statistics.

It is important that all realizations with $n_1 = 0$ and/or $n_2 = 0$ were discarded from the average. For small enough bin widths, $n_{1,2}$ took predominantly only two values (0 or 1), so all realizations with $\{n_1, n_2\} = \{1, 0\}, \{0, 1\}, \{0, 0\}$ were discarded. This procedure eliminated level correlations which would exhibit themselves in the enhanced probability, due to level repulsion, to detect configurations $\{1, 0\}$ and $\{0, 1\}$ compared to $\{1, 1\}$, if all configurations were counted. If only the realizations with $\{1, 1\}$ are counted in the ensemble averaging, the level correlations are eliminated by definition. Note that the function $K(\omega, \lambda)$ defined in Eq. (4) would correspond to averaging over all realizations of the sum of the products $\rho_1 \rho_2$ divided by the average of $n_1 n_2$ over all realizations.

The calculations of this section involve the numerical diagonalization of random matrices from the GRP ensemble of the *orthogonal* symmetry, in contrast to the analytical results of Sec. V derived for the *unitary* GRP. The similarity of the numerical results for $\tilde{K}(\omega, \lambda)$ to those derived analytically for $K(\omega, \lambda)$ corroborates the assumption of statistical independence of eigenfunctions and eigenvalues in GRP ensemble and demonstrates that there is no qualitative difference in the eigenfunction overlap statistics caused by the difference in symmetry class.

A. Diagonal drive

Here we present the results of numerical diagonalization of matrices described by Eq. (1), where $\widehat{H}_1$ is drawn from the GRP ensemble governed by Eqs. (8) and $\widehat{H}_2$ is an independently of $\widehat{H}_1$ fluctuating diagonal random matrix $\widehat{H}_2 = \text{diag}\{d'_n\}$ with the same variance of diagonal elements: $\langle d'^2_n \rangle = W^2$.

In Fig. 6, we plot the function $\tilde{K}(\omega, \lambda)$ obtained for $N = 1024$, $W = 1$, $\sigma^2 = 0.1 N^{-\gamma}$, $\gamma = 3/2$ and different values of λ. At a strong drive (the main plot), the results of numerical diagonalization are very similar to the prediction of the

Monthus surmise presented in Fig. 4. At a weak drive, the evolution of $\tilde{K}(\omega, \lambda)$ at small (fixed) ω is opposite to that of the strong drive due to the broadened self-correlation peak whose front is shifted to smaller values of ω as λ decreases (see Fig. 5).

It is instructive to extract the effective distribution $\mathcal{P}_\lambda(\Delta)$ of level shifts Δ in the LDoS defined by Eq. (36). At the scale $\Delta \gtrsim \Gamma$, this function gives the distribution of random shifts of the entire miniband in the LDoS, while at $\Delta \lesssim \delta$ it gives the distribution of random shifts of an individual level. To find $\mathcal{P}_\lambda(\Delta)$, we compute numerically the Fourier transform $G(t, \lambda)$ of $\tilde{K}(\omega, \lambda)$ and apply Eq. (36) performing the discrete (inverse) Fourier transform. The result is presented in Fig. 7 together with the corresponding analytical result obtained from Eqs. (4), (46), and (47). Note, however, that the analytical result is obtained for the unitary symmetry, while the numerics is done for the orthogonal symmetry, so only a qualitative agreement between Figs. 7(a) and 7(b) is expected.

B. Off-diagonal drive

When the diagonal matrix elements in Eq. (1) do not move, i.e., $\widehat{H}_2$ is an off-diagonal part of a matrix drawn from the GRP ensemble and $\widetilde{H}_1$ is an independently fluctuating full matrix from the same ensemble, the distribution function $\mathcal{P}_\lambda(\Delta)$ looks differently from the one at the diagonal drive. First, there is no shift of the miniband as a whole that manifests itself by the absence of the broad part of $\mathcal{P}_\lambda(\Delta)$ in Fig. 8. Remarkably, the shape of $\mathcal{P}_\lambda(\Delta)$ [obtained by Fourier transforming $G(t, \lambda)/G(t, 0)$ found by direct numerical calculations, see the inset to Fig. 8)] has the form of the Fermi distribution,

$$\mathcal{P}_\lambda(\Delta) = \frac{C}{1 + \exp[(|\Delta| - \mu)/T]}, \tag{64}$$
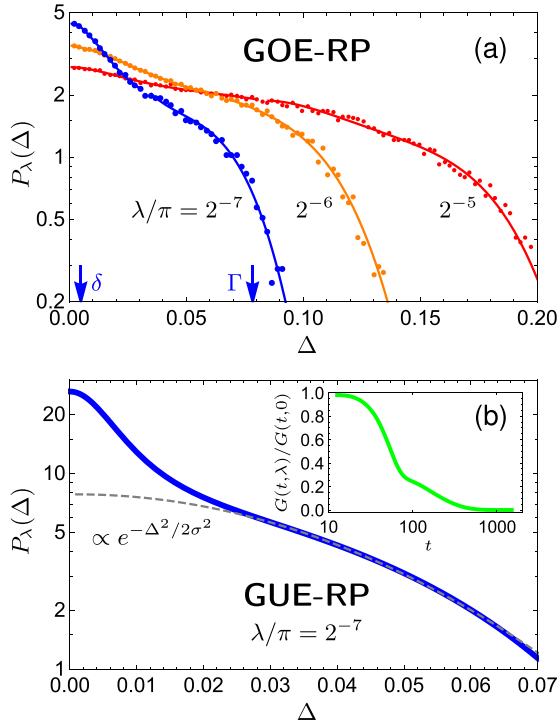
where $C^{-1} = 2T \ln(1 + e^{\mu/T}) \approx 2\mu$.

FIG. 7. Distribution of shifts in the local spectrum, $\mathcal{P}_\lambda(\Delta)$. (a) The result of numerical diagonalization of matrices from the orthogonal RP ensemble with $N = 1024$, $W = 1$, $\sigma^2 = N^{-\gamma}$, $\gamma = 3/2$ ($\Gamma/\delta = 32$), and $\lambda = \pi/128$, $\pi/64$, $\pi/32$. The Fourier transform $G(t, \lambda)$ of the EAO correlation function $\tilde{K}(\omega, \lambda)$ expressed in terms of eigenvectors and eigenvalues was computed directly and Fourier transformed according to Eq. (36). (b) The analytical result obtained by Fourier transforming $K(\omega, \lambda)$ given by Eqs. (4), (46), (47) and inverse Fourier transforming according to Eq. (36). The function $\mathcal{P}_\lambda(\Delta)$ consists of a narrow peak at small Δ [which reflects the broadened self-correlation peak in $K(\omega, \lambda)$, see the red curve in Fig. 5] on the top of a much broader distribution of the shifts of a miniband as a whole, see Fig. 1(a). The dashed line shows the Gaussian fit to this distribution. The similar features are seen in the numerical result (blue curve on the upper panel). Inset: The ratio $G(t, \lambda)/G(t, 0)$ whose inverse Fourier transform gives $\mathcal{P}_\lambda(\Delta)$.

In the main plot of Fig. 8, the numerical result for $\mathcal{P}_\lambda(\Delta)$ is shown by a purple curve and the orange dashed line is the fit by Eq. (64). As one can see, the fit is almost perfect. As λ decreases, the width μ of the distribution and the effective temperature T both decrease but the ratio T/μ remains small and is likely to vanish in the limit $\lambda \to 0$. This behavior is similar to the one obtained analytically for the diagonal drive and shown in Fig. 5, but in contrast to the diagonal drive, the Lorentzian tail is absent at the off-diagonal drive.

To estimate the expected width of the distribution $\mathcal{P}_\lambda(\Delta)$, one can use Eq. (55) derived for the diagonal drive in which the driving force, the variance $\langle d'^2 \rangle$, should be replaced by $\sum_m \langle (H_{2,nm})^2 \rangle = N\sigma^2 \propto N^{1-\gamma}$. Then the parameter α transforms to

$$\alpha_{\text{off}} = \lambda^2 N/2, \tag{65}$$

and using Eq. (63), we obtain

$$\Delta E_n \equiv \mu \sim \delta \left(\lambda \sqrt{N}\right) \sim \lambda W N^{-1/2}. \tag{66}$$
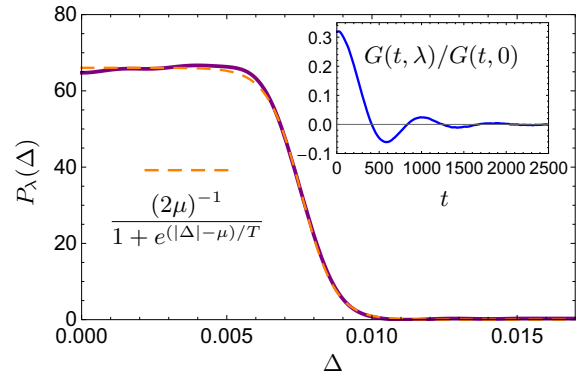

FIG. 8. $\mathcal{P}_\lambda(\Delta)$ for the off-diagonal drive. The result of numerical diagonalization for the orthogonal RP ensemble with $N = 1024$, $W = 1$, $\sigma^2 = N^{-\gamma}$, $\gamma = 3/2$ and $\lambda = \pi/128$. The solid purple curve is the Fourier transform according to Eq. (36) of $G(t, \lambda)/G(t, 0)$ found from exact diagonalization and shown in the inset. The dashed orange line is the fit to the Fermi-like function (64) with $\mu = 0.00757$ and $T = 0.000585$.

Hence the typical shift of the level μ for the off-diagonal drive in the fractal phase ($1 < \gamma < 2$) is independent of γ.

Finally, we present the numerical results for the sensitivity of the EAO correlation function $\delta\tilde{K}(\delta, \lambda)$ at a scale $\omega = \delta$ to the change of the control parameter λ for the off-diagonal drive. To this end, we define the EAO susceptibility according to

$$\chi_{\text{EAO}} = \frac{\tilde{K}(\delta, \lambda) - \tilde{K}(\delta, 0)}{\lambda^2}. \tag{67}$$

Figure 9 demonstrates that it has the same shape as the fidelity susceptibility shown in Fig. 1(b) and its scaling with the matrix size N differs only by a γ-independent extra factor of N. This extra factor can be easily understood if we evaluate the numerator in Eq. (67) expanding the functions $F(\pi, \alpha)$ [Eq. (53)] and $\Phi(\pi, \alpha)$ [Eq. (59)] to the first order in α and
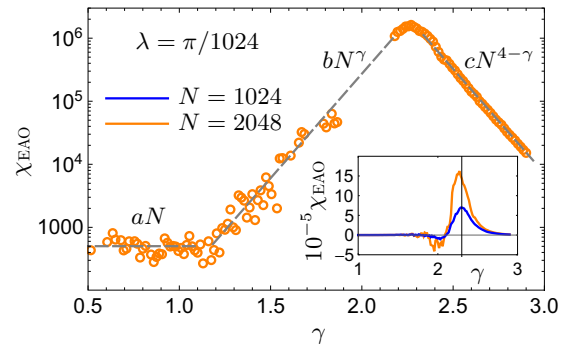

FIG. 9. Eigenfunction overlap susceptibility defined by Eq. (67) and obtained from the numerical diagonalization as a function of γ. Its scaling with N is determined by Eqs. (69) and (37), as indicated on the plot. The shift of the maximum away from $\gamma_{\text{AT}} = 2$ is a finite-size effect (see text). Inset: χ_{EAO} in a linear scale for $N = 1024$ and $N = 2048$, showing a shift of the maximum closer to γ_{AT} with increasing N.

replacing the latter by α_{off}:

$$K(\delta, \lambda) - K(\delta, 0) \sim K(\delta, 0)\,\alpha_{\text{off}} \sim \chi_F^{(\text{typ})}\,\alpha_{\text{off}}. \qquad (68)$$

Now taking α_{off} from Eq. (65), we obtain

$$\chi_{\text{EAO}} \sim N\chi_F^{(\text{typ})}. \qquad (69)$$

This similarity (confirmed numerically in Fig. 9) implies that not only the leading in λ^2 correction to the fidelity, $1 - F^2 \approx \lambda^2 \chi_F^{(\text{typ})}$, but also the next in λ^2 correction, $\lambda^2[K(\delta, \lambda) - K(\delta, 0)] = \lambda^4 \chi_{\text{EAO}}$ as functions of γ are peaked at the localization transition. The apparent shift of the maximum $\gamma_{\max}$ away from the transition point $\gamma_{\text{AT}} = 2$ is a finite-size effect. Indeed, with the constants $b, c \sim 1$ defined in Fig. 9, one finds a correction $(1/2)\ln(c/b)/\ln N \sim 15\%$ to $\gamma_{\max}$. A similar correction would appear for $\gamma_{\max}$ in $\chi_F^{(\text{typ})}$ if the corresponding prefactors $\tilde{b}$ and $\tilde{c}$ are taken into account in Eq. (37). Taking the log derivative as in Eq. (39) eliminates this correction and brings $\gamma_{\max}$ almost exactly to γ_{AT}, see Fig. 1(b). Unfortunately, strong data scattering makes this operation impossible for χ_{EAO}.

Equation (69) may be considered as a numerical justification of the replacement $\alpha \to \alpha_{\text{off}}$, with α_{off} given by Eq. (65), for the small-λ expansion of fidelity F in the case of the off-diagonal drive.

VII. CONCLUSION

In this paper, we studied the response of an isolated quantum system governed by the GRP random matrix Hamiltonian $\widehat{H}_1$ to a perturbation $\lambda\widehat{H}_2$. In contrast to the disordered spin chains, where a complete analytical treatment was not possible so far, our random matrix model can be exactly solved in the region of ergodic and fractal states by the formalism of the Efetov's supersymmetric NLSM in the thermodynamic limit $N \to \infty$. This solution has a natural extension to the region of localized states which is successfully tested numerically.

In this paper, we obtained asymptotically exact expressions, Eqs. (46) and (47), for the DoS and LDoS correlation functions in the GRP ensemble of unitary symmetry in its fractal phase. Having calculated the EAO correlation function given by Eq. (4), we compared it with a simple analytical treatment based on the Monthus surmise [Eq. (13)], as well as with the numerical simulations on the orthogonal-symmetry version of the same ensemble. The studied correlation functions behave qualitatively in the same way for both symmetries. We identified analytically the parameter α [Eqs. (55) and (65) for different types of drives], which controls a typical shift of individual levels by a small perturbation of the Hamiltonian.

We focus on the typical fidelity susceptibility $\chi_F^{(\text{typ})}$ [Eq. (6)] and the susceptibility of the EAO χ_{EAO} [Eqs. (67) and (5)] to such a perturbation. We show that $\chi_F^{(\text{typ})}$ and χ_{EAO} contain essentially the same information on the effect of the perturbation on the eigenfunction overlap.

It is demonstrated both analytically and numerically that these susceptibilities as functions of the effective disorder parameter γ are strongly peaked near the localization transition: they are nearly constant in the ergodic phase, increase exponentially in the fractal phase, and decrease exponentially
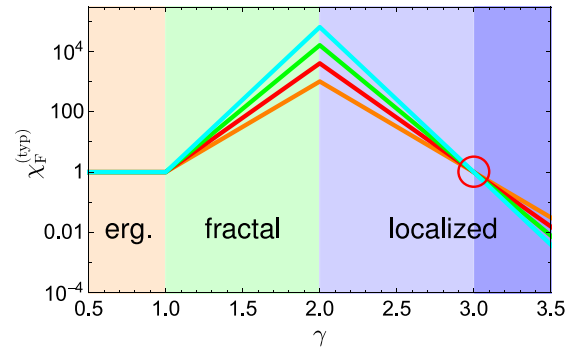

FIG. 10. Sketch of the fidelity susceptibility as a function of the effective disorder parameter γ at different system sizes (from orange to cyan in increasing N order) in the thermodynamic limit, $N \to \infty$. For finite N, χ_F^{typ} acquires γ-dependent corrections rounding the curves and shifting the maximum, as in Fig. 9. The plot corresponds to Fig. 1(b) and should be compared with Fig. 1 in Ref. [35].

in the localized phase. Furthermore, in the localized phase we identified two drastically different regimes of the behavior of $\chi_F^{(\text{typ})} \sim \chi_{\text{EAO}}/N$ with increasing the matrix size N (which is the dimension of the Hilbert space in this problem). Both susceptibilities grow with N for $2 < \gamma < 3$ and decrease with N for $\gamma > 3$, with a fixed point at $\gamma^* = 3$.

The overall behavior of $\chi_F^{(\text{typ})}$ sketched in Fig. 10 is very similar to the one for the scaled typical normalized fidelity susceptibility of a true many-body system, the disordered XXZ spin chain, studied recently by Sels and Polkovnikov [35]. This similarity also includes the existence of an apparent fixed point that separates the regimes of increasing and decreasing $\chi_F^{(\text{typ})}$ with the Hilbert space dimension N. We argue that the first regime is realized when two resonant localized states may hybridize and form the Mott's pair of bonding and antibonding states with the level splitting $\Delta E \sim \delta$. The second regime implies that such double-headed states are rare and make a subleading contribution compared to typical single-headed ones.

We believe that the similarity of our Fig. 1(b) and Fig. 1 of Ref. [35] is not accidental, reflecting the common physics both in the many-body problem of disordered spin chains and in the RP random matrix problem.

APPENDIX: DERIVATION OF EQS. (46), (47) BY THE EFETOV'S NLSM FORMALISM

In this Appendix, we outline the main steps in the derivation of the analytical results (46) and (47) for the DoS and LDoS parametric correlation functions in the fractal phase of the unitary GRP model subject to the diagonal drive. The details will be reported elsewhere [43].

We take the variance of off-diagonal elements of the Hamiltonian in Eqs. (8) to be $\sigma^2 = 1/N$. Then the fractal nonergodic phase is realized for $1 \ll W^2 \ll N$. In terms of the energy scales, that corresponds to the hierarchy $\delta \ll \Gamma \ll E_{\mathrm{BW}} \sim W$, see Table I.

To simplify calculations, it is convenient to write the GRP Hamiltonian as a sum of a totally basis-invariant RMT part and a diagonal contribution,

$$H(\lambda) = H_{\mathrm{RMT}} + \widehat{d}\cos\lambda + \widehat{d'}\sin\lambda, \qquad (A1)$$

where H_{RMT} is a random matrix from the Gaussian unitary ensemble with the variance of all (including diagonal) elements $\langle |H_{nm}|^2 \rangle = 1/N$, while $\widehat{d} = \mathrm{diag}(d_n)$ and $\widehat{d'} = \mathrm{diag}(d'_n)$ are diagonal matrices independently distributed with zero mean and $\langle d_n^2 \rangle = \langle d_n'^2 \rangle = W^2 - 1/N$ (since the variance of a sum of normally distributed random variables is additive). In the fractal phase, the last $(1/N)$ term is negligible that will be assumed hereafter.

In the self-consistent Born approximation, justified in the fractal phase since $\Gamma \gg \Delta$, the average Green's function is given by

$$\langle G_{ij}^{\mathrm{R,A}}(E, \lambda) \rangle = \frac{\delta_{ij}}{E \pm i\Gamma/2}, \qquad (A2)$$

where the width is obtained by Fermi's golden rule: $\Gamma = 2\pi \langle |H_{ij}|^2 \rangle / \delta$, in accordance with Table I.

The DoS and LDoS correlation functions [Eqs. (2) and (3)] can be expressed in terms of the average product of the retarded and advanced Green's functions calculated at different values of the control parameter λ:

$$Y_{rs}(\omega, \lambda) = \langle G_{rr}^{\mathrm{R}}(E + \omega/2, -\lambda/2) G_{ss}^{\mathrm{A}}(E - \omega/2, \lambda/2) \rangle. \qquad (A3)$$

In the RP model, the matrix Y_{rs} is characterized by two parameters: its diagonal (Y_{rr}) and off-diagonal ($Y_{r \neq s}$) elements. They determine the correlators in question:

$$R(\omega, \lambda) = \frac{1}{2} + \frac{\delta^2}{2\pi^2} \mathrm{Re}\left[N(N-1) Y_{r \neq s} + N Y_{rr} \right], \qquad (A4)$$

$$C(\omega, \lambda) = \frac{1}{2} + \frac{N^2 \delta^2}{2\pi^2} \mathrm{Re}\, Y_{rr}. \qquad (A5)$$

To perform the average in Eq. (A3), we follow the standard Efetov's formalism of the supersymmetric NLSM [15], repeating the sequence of routine steps: representation of the Green's function via integrals over supervectors ψ, averaging over the GUE matrix H_{RMT}, decoupling the resulting quartic-in-ψ term by the Hubbard-Stratonovich transformation that introduces a 4×4 supermatrix Q acting in the tensor product of the superspace (FB) and retarded-advanced (RA) space, and taking the final Gaussian integral over ψ. We also add a symmetry-breaking source term to the action, $J = \mathrm{diag}\{J_i\}$, where $J_i = \mathrm{diag}(\xi_i^{\mathrm{R}}, \xi_i^{\mathrm{A}}) \otimes \widehat{P}_{\mathrm{B}}$ and $\widehat{P}_{\mathrm{B}}$ projects onto the BB

sector, and define the partition function:

$$Z[J] = \int e^{S[Q,J]} DQ. \qquad (A6)$$

Then the correlator (A3) is expressed as

$$Y_{rs} = \frac{\partial^2 Z[J]}{\partial \xi_r^{\mathrm{R}} \partial \xi_s^{\mathrm{A}}} \bigg|_{\xi=0}. \qquad (A7)$$

A new ingredient in this standard RMT scheme arising for the RP model is the presence of diagonal disorder in Eq. (A1) that requires additional averaging. However, since after the Hubbard-Stratonovich transformation different components of the supervector ψ_i $(i = 1, \ldots, N)$ are already decoupled and both disorder ($\widehat{d}$ and $\widehat{d'}$) and the source J are also diagonal, each component can still be averaged independently. The action then is given by

$$S[Q, J] = -\frac{N\Gamma^2}{8} \mathrm{str}\, Q^2 + S_\sigma[Q, J], \qquad (A8)$$

where the last term is obtained as a sum of N independent contributions (assuming the band center, $E = 0$, and linearizing for small λ):

$$S_\sigma[Q, J] = \sum_{i=1}^{N} \ln \langle \mathrm{sdet}(\tilde{\omega}\Lambda/2 - d + i\Gamma Q/2 + J_i) \rangle_{d, d'}. \qquad (A9)$$

Here averaging is performed over two independent Gaussian variables d and d' (initially, ith components of $\widehat{d}$ and $\widehat{d'}$), both with the variance W^2. Note that d' responsible for the drive enters the action Eq. (A9) via a frequency shift

$$\tilde{\omega} = \omega - \lambda d', \qquad (A10)$$

as follows from the structure of the arguments of the Green's functions in Eq. (A3).

At $\omega = 0$, $\lambda = 0$, and in the absence of sources ($J = 0$), the action (A8) does not involve any nontrivial matrices rather than Q (d enters with the unit matrix in the FB $\otimes$ RA space) and therefore possesses a degenerate manifold of saddle points $Q = U^{-1}\Lambda U$ spanning the coset $\mathrm{U}(2|2)/\mathrm{U}(1|1) \times \mathrm{U}(1|1)$. The action of the resulting NLSM is given by Eq. (A9).

Since we are interested in the parametric statistics at small values of the control parameter $\lambda \ll 1$, the roles of d and d' averaging are essentially different. The former provides the leading contribution responsible for the formation of the miniband, whereas the latter describes parametric correlations in the spectrum.

In the absence of sources, the NLSM action (A9) depends only on Cartan variables, coinciding with λ_{F} and λ_B in the Efetov's parametrization [15]. Then,

$$\mathrm{sdet}(\omega\Lambda/2 - d + i\Gamma Q/2) = \frac{4d^2 + \tilde{M}_{\mathrm{F}}}{4d^2 + \tilde{M}_{\mathrm{B}}}, \qquad (A11)$$

where we introduced a short-hand notation:

$$\tilde{M}_{\mathrm{F,B}} = \Gamma^2 - \tilde{\omega}^2 - 2i\Gamma\tilde{\omega}\lambda_{\mathrm{F,B}}. \qquad (A12)$$

Averaging the superdeterminant over d, we obtain the source-free action $S \equiv S[Q, 0]$ given by Eq. (48).

Calculation of the derivatives in Eq. (A7) is performed in the Efetov's parametrization, which contains four real variables (two Cartan coordinates, $\lambda_{F,B}$, and two angular variables) and four Grassmann numbers. After some algebra [43], we obtain in the leading order in $N \to \infty$,

$$Y_{r \neq s} = \frac{\pi^2}{N^2 \delta^2} \int DQ \big[1 + (\lambda_B - \lambda_F)^2 P_R G_4 \big] e^S, \qquad \text{(A13)}$$

$$Y_{rr} = \frac{2\pi}{N \delta \Gamma} \int DQ \bigg[\bigg\langle \frac{\Gamma}{\Gamma - i\tilde{\omega}} \bigg\rangle_{d'} + (\lambda_B - \lambda_F) P_C G_4 \bigg] e^S, \qquad \text{(A14)}$$

where angular brackets stand for averaging over d', the functions $P_R(\lambda_B)$ and $P_C(\lambda_B)$ defined in Eqs. (49) and (50) also

involve averaging over d', and G_4 is the product of all four Grassmann variables.

The invariant measure for integration over the manifold of Q matrices is given by [15]

$$\int DQ \cdots = \int_{-1}^{1} d\lambda_F \int_{1}^{\infty} d\lambda_B \frac{dG}{(\lambda_B - \lambda_F)^2} \cdots, \qquad \text{(A15)}$$

where dG stands for the measure over four Grassmann variables (we omit integration over two angular coordinates since the integrand does not depend on them). After integration over dG in Eqs. (A13) and (A14), the term G_4 gives unity and various combinations of two Grassmann variables vanish (therefore they are omitted in those equations), while the Grassmann-free terms do contribute due to the singularity of the measure at $\lambda_F = \lambda_B = 1$ (Efetov-Wegner boundary term [15]). Collecting altogether, we arrive at Eqs. (46) and (47).

---

[1] M. L. Mehta, *Random Matrices* (Elsevier, Amsterdam, 2004).

[2] D. J. Thouless, Electrons in disordered systems and the theory of localization, Phys. Rep. **13**, 93 (1974).

[3] M. Wilkinson, Random matrix theory in semiclassical quantum mechanics of chaotic systems, J. Phys. A: Math. Gen. **21**, 1173 (1988).

[4] V. E. Kravtsov and M. R. Zirnbauer, Kramers degeneracy and quantum jumps in the persistent current of disordered metal rings, Phys. Rev. B **46**, 4332 (1992).

[5] B. D. Simons and B. L. Altshuler, Universal Velocity Correlations in Disordered and Chaotic Systems, Phys. Rev. Lett. **70**, 4063 (1993).

[6] A. Szafer and B. L. Altshuler, Universal Correlation in the Spectra of Disordered Systems with an Aharonov-Bohm Flux, Phys. Rev. Lett. **70**, 587 (1993).

[7] B. D. Simons, P. A. Lee, and B. L. Altshuler, Exact Description of Spectral Correlators by a Quantum One-Dimensional Model with Inverse-Square Interaction, Phys. Rev. Lett. **70**, 4122 (1993).

[8] J. Zakrzewski and D. Delande, Parametric motion of energy levels in quantum chaotic systems. I. Curvature distributions, Phys. Rev. E **47**, 1650 (1993).

[9] F. von Oppen, Exact Distribution of Eigenvalue Curvatures of Chaotic Quantum Systems, Phys. Rev. Lett. **73**, 798 (1994).

[10] I. M. Khaymovich, V. E. Kravtsov, B. L. Altshuler, and L. B. Ioffe, Localization transition on the random regular graph as an unstable tricritical point in a log-normal Rosenzweig-Porter random matrix ensemble, arXiv:2002.02979.

[11] I. M. Khaymovich and V. E. Kravtsov, Dynamical phases in a "multifractal" Rosenzweig-Porter model, SciPost Phys. **11**, 045 (2021).

[12] K. S. Tikhonov and A. D. Mirlin, Eigenstate correlations around many-body localization transition, Phys. Rev. B **103**, 064204 (2021).

[13] A. V. Andreev and B. L. Altshuler, Spectral Statistics Beyond Random Matrix Theory, Phys. Rev. Lett. **75**, 902 (1995).

[14] I. V. Yurkevich and V. E. Kravtsov, Non-Universal Corrections to the Level Curvature Distribution Beyond Random Matrix Theory, Phys. Rev. Lett. **78**, 701 (1997).

[15] K. Efetov, *Supersymmetry in Disorder and Chaos* (Cambridge University Press, Cambridge, 1996).

[16] F. J. Dyson, A Brownian-motion model for the eigenvalues of a random matrix, J. Math. Phys. **3**, 1191 (1962).

[17] P. Pechukas, Distribution of Energy Eigenvalues in the Irregular Spectrum, Phys. Rev. Lett. **51**, 943 (1983).

[18] F. Evers and A. D. Mirlin, Anderson transitions, Rev. Mod. Phys. **80**, 1355 (2008).

[19] J. T. Chalker, I. V. Lerner, and R. Smith, Random Walks through the Ensemble: Linking Spectral Statistics with Wave-Function Correlations in Disordered Metals, Phys. Rev. Lett. **77**, 554 (1996).

[20] J. T. Chalker, V. E. Kravtsov, and I. V. Lerner, Spectral rigidity and eigenfunction correlations at the Anderson transition, Pis'ma v Zh. Eksp. Teor. Fiz. **64**, 355 (1996) [JETP Lett. **64**, 386 (1996)].

[21] N. Macé, F. Alet, and N. Laflorencie, Multifractal Scalings Across the Many-Body Localization Transition, Phys. Rev. Lett. **123**, 180601 (2019).

[22] M. Tarzia, Many-body localization transition in Hilbert space, Phys. Rev. B **102**, 014208 (2020).

[23] V. E. Kravtsov, I. M. Khaymovich, and M. Amini, A random matrix model with localization and ergodic transitions, New J. Phys. **17**, 122002 (2015).

[24] N. Rosenzweig and C. E. Porter, "Repulsion of energy levels" in complex atomic spectra, Phys. Rev. **120**, 1698 (1960).

[25] V. N. Smelyanskiy, K. Kechedzhi, S. Boixo, S. V. Isakov, H. Neven, and B. L. Altshuler, Non-Ergodic Delocalized States for Efficient Population Transfer within a Narrow Band of the Energy Landscape, Phys. Rev. X **10**, 011017 (2020).

[26] L. Faoro, M. V. Feigel'man, and L. B. Ioffe, Non-ergodic phase of the quantum random energy model, Ann. Phys. **409**, 167916 (2019).

[27] I. M. Khaymovich, V. E. Kravtsov, B. L. Altshuler, and L. B. Ioffe, Fragile ergodic phases in logarithmically-normal Rosenzweig-Porter model, Phys. Rev. Research **2**, 043346 (2020).

[28] A. De Luca, B. L. Altshuler, V. E. Kravtsov, and A. Scardicchio, Anderson Localization on the Bethe Lattice: Nonergodicity of Extended States, Phys. Rev. Lett. **113**, 046806 (2014).

[29] K. S. Tikhonov, A. D. Mirlin, and M. A. Skvortsov, Anderson localization and ergodicity on random regular graphs, Phys. Rev. B **94**, 220203(R) (2016).

[30] K. S. Tikhonov and A. D. Mirlin, From Anderson localization on random regular graphs to many-body localization, Ann. Phys. **435**, 168525 (2021).

[31] E. Cuevas and V. E. Kravtsov, Two-eigenfunction correlation in a multifractal metal and insulator, Phys. Rev. B **76**, 235119 (2007).

[32] G. De Tomasi, M. Amini, S. Bera, I. M. Khaymovich, and V. E. Kravtsov, Survival probability in generalized Rosenzweig-Porter random matrix ensemble, SciPost Phys. **6**, 014 (2019).

[33] W.-L. You, Y.-W. Li, and S.-J. Gu, Fidelity, dynamic structure factor, and susceptibility in critical phenomena, Phys. Rev. E **76**, 022101 (2007).

[34] W.-L. You and L. He, Generalized fidelity susceptibility at phase transitions, J. Phys.: Condens. Matter **27** (2015).

[35] D. Sels and A. Polkovnikov, Dynamical obstruction to localization in a disordered spin chain, Phys. Rev. E **104**, 054105 (2021).

[36] N. F. Mott, Conduction in non-crystalline systems. I. Localized electronic states in disordered systems, Philos. Mag. **17**, 1259 (1968).

[37] N. F. Mott, Conduction in non-crystalline systems. IV. Anderson localization in a disordered lattice, Philos. Mag. **22**, 7 (1970).

[38] D. A. Ivanov, M. A. Skvortsov, P. M. Ostrovsky, and Y. V. Fominov, Hybridization of wave functions in one-dimensional localization, Phys. Rev. B **85**, 035109 (2012).

[39] G. Biroli and M. Tarzia, Lévy-Rosenzweig-Porter random matrix ensemble, Phys. Rev. B **103**, 104205 (2021).

[40] E. Bogomolny and M. Sieber, Eigenfunction distribution for the Rosenzweig-Porter model, Phys. Rev. E **98**, 032139 (2018).

[41] C. Monthus, Multifractality of eigenstates in the delocalized non-ergodic phase of some random matrix models: Wigner-Weisskopf approach, J. Phys. A: Math. Theor. **50**, 295101 (2017).

[42] V. Weisskopf and E. Wigner, Berechnung der natürlichen Linienbreite auf Grund der Diracschen Lichttheorie, Z. Phys. **63**, 54 (1930).

[43] M. A. Skvortsov and V. E. Kravtsov, Parametric statistics in the Rosenzweig-Porter model (unpublished).